CHAPTER VI

Investigation of AC Conductivity and Electric Modulus of $Bi_{4-x}Me_xV_2O_{11-\delta}$ (Me = Ca, Li, Ba) Solid Solutions

---

Until man duplicates a blade of grass, nature can laugh at his so-called scientific knowledge.

Thomas A. Edison

6.1 Introduction:

Impedance Spectroscopy (IS) has been extensively used to measure and analyze the response from the electrode and electrolyte as well as the interface. Initially, this method was applied to the determination of the double-layer capacitance [**1-4**]. IS studies the system response to the application of a periodic small amplitude ac signal and the measurements are carried out at different ac frequencies. Analysis of the system response contains information about the interface, its structure and reactions taking place there. The different individual elements (R, C and L) representing the electrochemical processes in the material are frequency dependent and possess different relaxation times due to various processes **[5, 6-7]**. This chapter briefly describes the temperature dependent ac conductivity and electric modulus studies to understand ion dynamics of Li, Ca and Ba substituted bismuth vanadate. For better clarity, all the graphs are plotted in logarithmic scale.

6.2 Experimental

Polycrystalline ceramic samples of pure and doped $Bi_{4-x}Me_xV_2O_{11-\delta}$ (Me = Ca, Li, Ba) series of compounds have been synthesized by standard solid state reaction method. The details procedure for the preparation of pelletized samples had been discussed in **chapters II**.

6.3 Results and discussion

6.3.1 Frequency dependent conductivity

The ac conductivity is calculated from the measured real & imaginary parts of the impedance data and pellet dimensions for the samples of the series of compounds $Bi_{4-x}Ca_xV_2O_{11-\delta}$, $Bi_{4-x}Li_xV_2O_{11-\delta}$ and $Bi_{4-x}Ba_xV_2O_{11-\delta}$. **Fig. 6.1 (a-g)** show the frequency dependence of conductivity at various temperatures for the highest and lowest dopant compositions along with the parent compound (x = 0) of the three series of compounds.

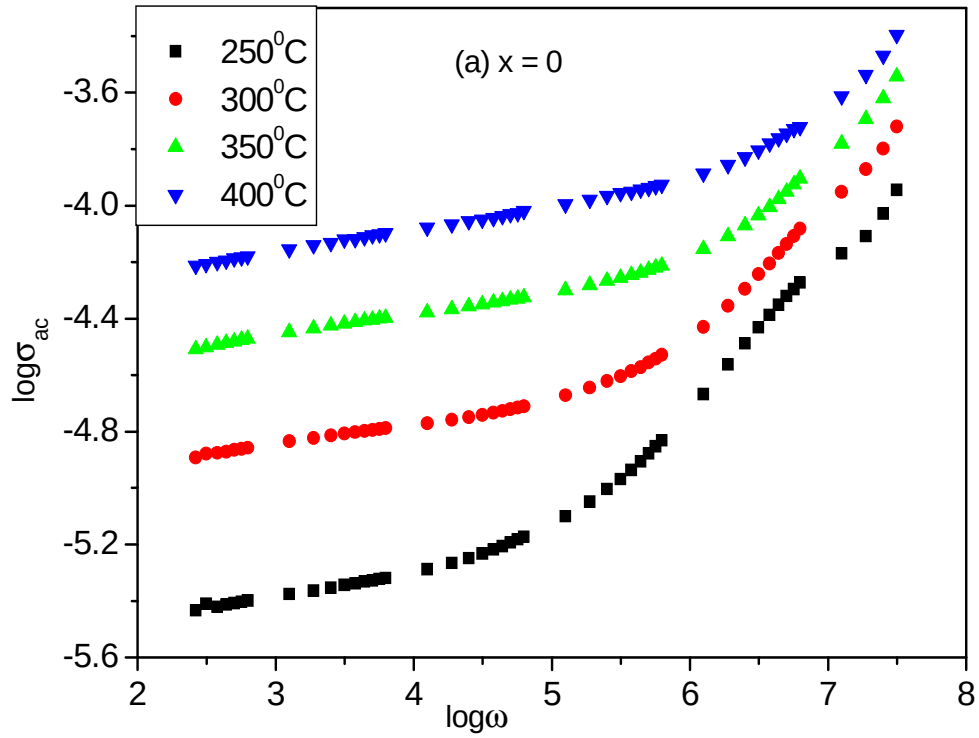

Fig.6.1 (a) Log ω vs, log σ_{ac} plots for the parent compound $Bi_4V_2O_{11}$ at different temperatures.

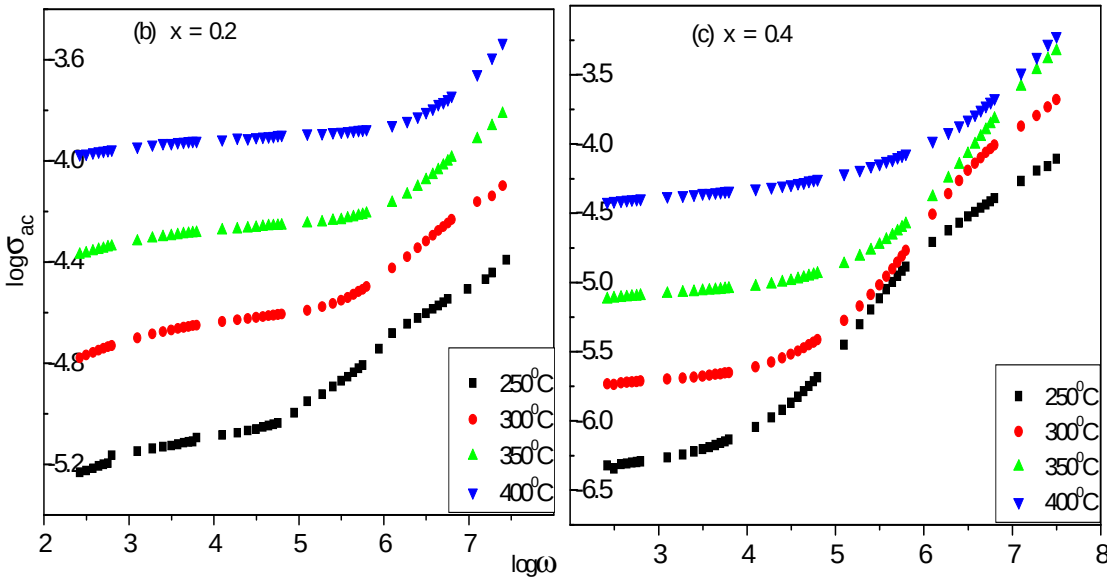

Fig.6.1 (b, c): Log ω vs, log σ_{ac} plots for (b) highest conducting (x = 0.2) and (c) lowest conducting (x = 0.4) dopant compositions of $Bi_{4-x}Ca_xV_2O_{11-\delta}$ at different temperatures.

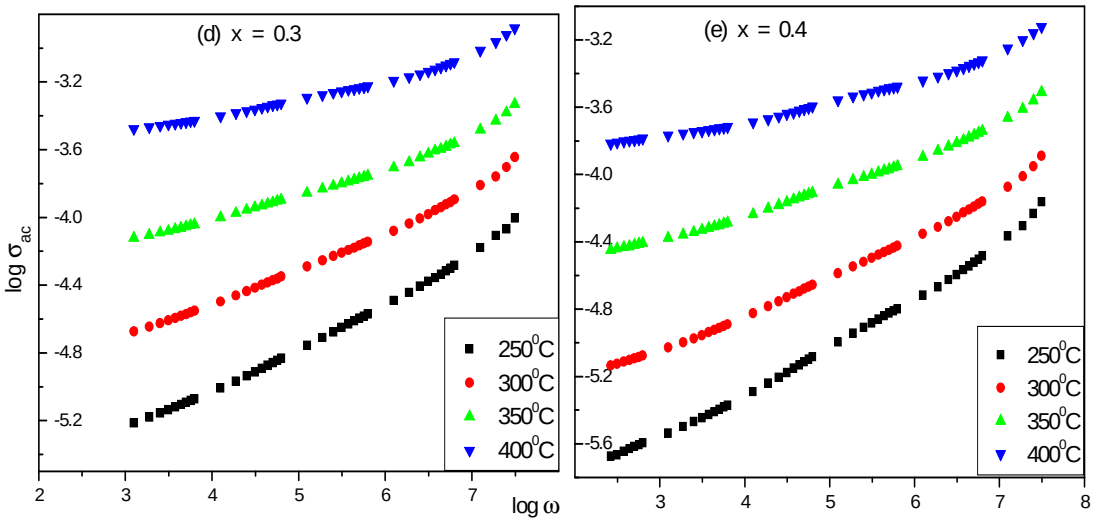

Fig.6.1 (d, e): Log ω vs, log σ_{ac} plots for (d) highest conducting (x = 0.3) and (e) lowest conducting (x = 0.4) dopant compositions of $Bi_{4-x}Ba_xV_2O_{11-\delta}$ at different temperatures.

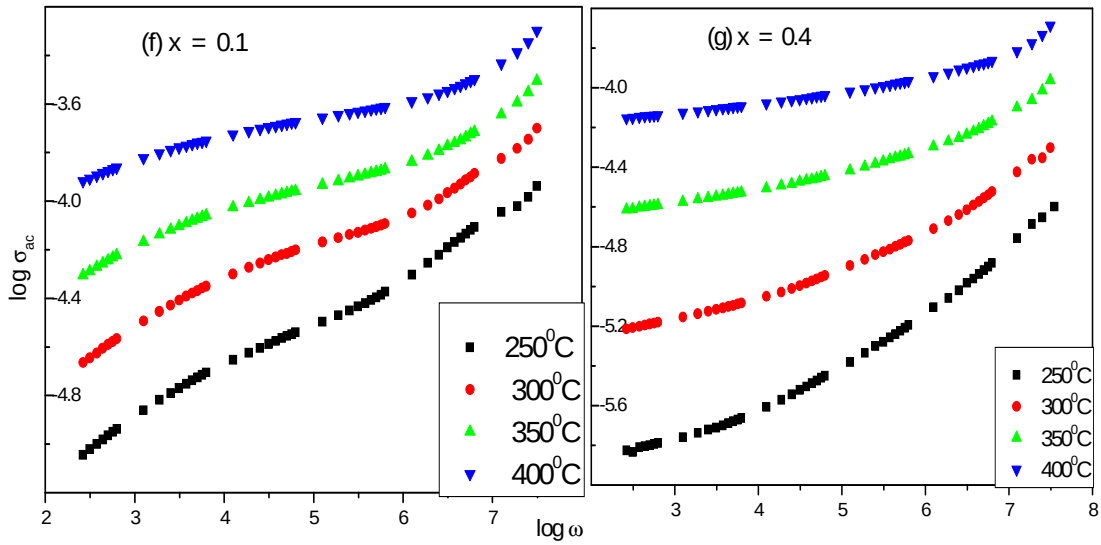

Fig.6.1 (f, g): Log ω vs, log σ_{ac} plots for (f) highest conducting and (g) lowest conducting dopant compositions of $Bi_{4-x}Li_xV_2O_{11-\delta}$ at different temperatures.

It is noticeable that, for both pure and doped compounds the ac conductivity plots show three distinct regime a) low frequency dispersed b) an intermediate plateau and c) conductivity dispersion at high frequency which is a typical frequency dependent conductivity spectrum exhibited by solid electrolyte [**7--10**). At very low frequencies, more and more charges are accumulated at the electrode-electrolyte interface and as a result drop in conductivity is observed. In the intermediate frequency plateau region,

the conductivity (σ_0) is found to be frequency independent and is almost equal to dc conductivity which originates from the random diffusion of the charge carriers through activated hopping. At the high frequency region, the conductivity increases with frequency. The σ_0 obtained on extrapolation to lower frequencies and found to be in good agreement with the dc conductivity obtained from the impedance analysis. In the **Fig**. **6.1(a-g)** of $\log \sigma_{ac}$ vs. log ω plots, the frequency at which the dispersion region starts from the dc conductivity plateau can be defined as the characteristic frequency (ω_0), where the relaxation effects of the ions occur. This characteristic frequency is termed as hopping frequency or cross over frequency [**7**]. With rise in temperature, the hopping frequency, i.e. the frequency at which the conductivity begins to disperse, shifts towards the higher frequency. In the conductivity plot, a little deviation from σ_{dc} observed in the plateau region is a sign of electrode polarization. As temperature increases, the low frequency electrode polarization effect become more pronounced and thereby the plateau region and hence the hopping frequency shifts towards the higher frequency region. The frequency dependence of conductivity in the dispersive regions for all the compositions of the compounds $Bi_4V_2O_{1,}$ $Bi_{4-x}Ca_xV_2O_{11-\delta}$, $Bi_{4-x}Li_xV_2O_{11-\delta}$ and $Bi_{4-x}Ba_xV_2O_{11-\delta}$ at various temperatures were analyzed using the Universal Jonscher's power law [**10-13**],

$$\sigma_{ac} = \sigma_0 + A\omega^n \qquad (6.1)$$

Where, σ_{ac} is the ac conductivity, σ_o is the frequency independent conductivity corresponding to the plateau region, *A* is a pre-exponential factor, ω = $2\pi f$ is the angular frequency and *n* is the power law exponent related with the degree of interaction among the moving ions and the surrounding. For ionic conductors, generally the value of the exponent ranges between 0.5 and 0.1 [**12, 14**]. The value of the power law exponent calculated for the high conducting compositions x = 0.2, x = 0.3 and x = 0.1 of the compounds $Bi_{4-x}Ca_xV_2O_{11-\delta}$, $Bi_{4-x}Li_xV_2O_{11-\delta}$ and $Bi_{4-x}Ba_xV_2O_{11-\delta}$ along with the undoped compound $Bi_4V_2O_{11}$ are shown in **Fig. 6.2.** In our study the value of n ranges between 0.58 and 0.89 which is in the range of ionic conductor.

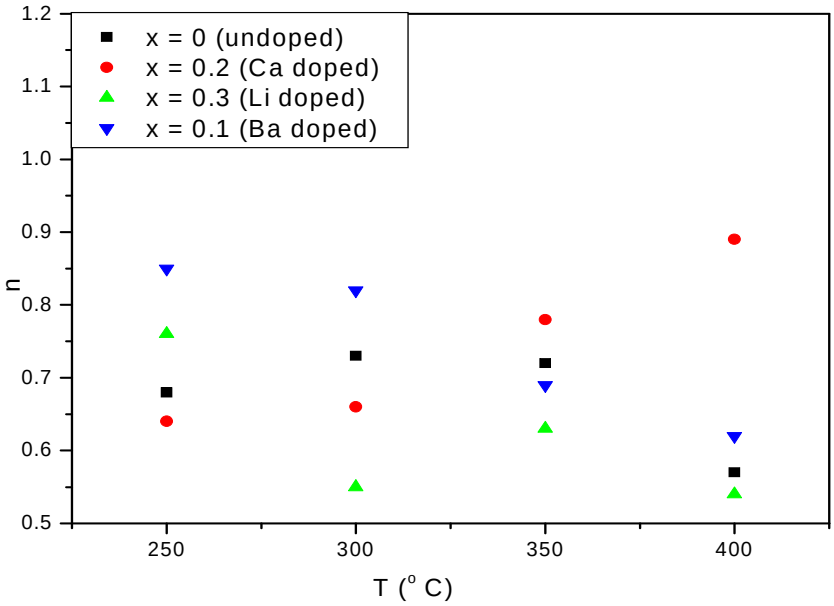

Fig. 6.2: Temperature dependence of power law exponent (n) obtained the parent as well as the high conducting samples of the doped series of compounds.

Fig. 6.3 (a-g) shows the scaled behaviour of the frequency dependent conductivity, i.e., log (σ_{ac}/σ_0) vs log (ω/ω_0) plots at various temperatures, where ω_0 is the hopping frequency. For all compositions, the scaled plot at different temperatures almost merges to a single curve. The merging of log (σ_{ac}/σ_0) vs log (ω/ω_0) curves at various temperatures suggests that the conductivity relaxation mechanism in these compounds is found to be temperature independent [**15**].

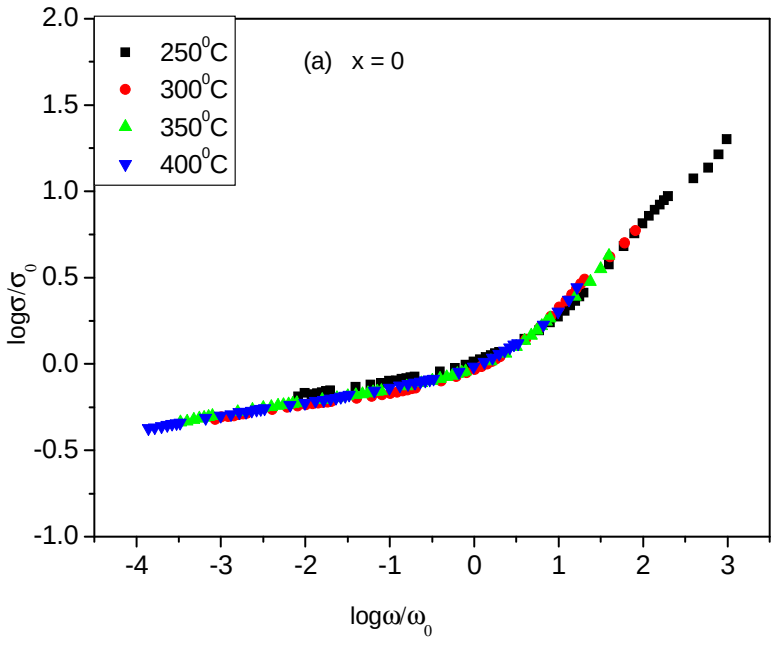

Fig.6.3 (a) Log ω/ω_0 vs, log σ_{ac}/σ_0 plots for the parent compound $Bi_4V_2O_{11}$ at different temperatures.

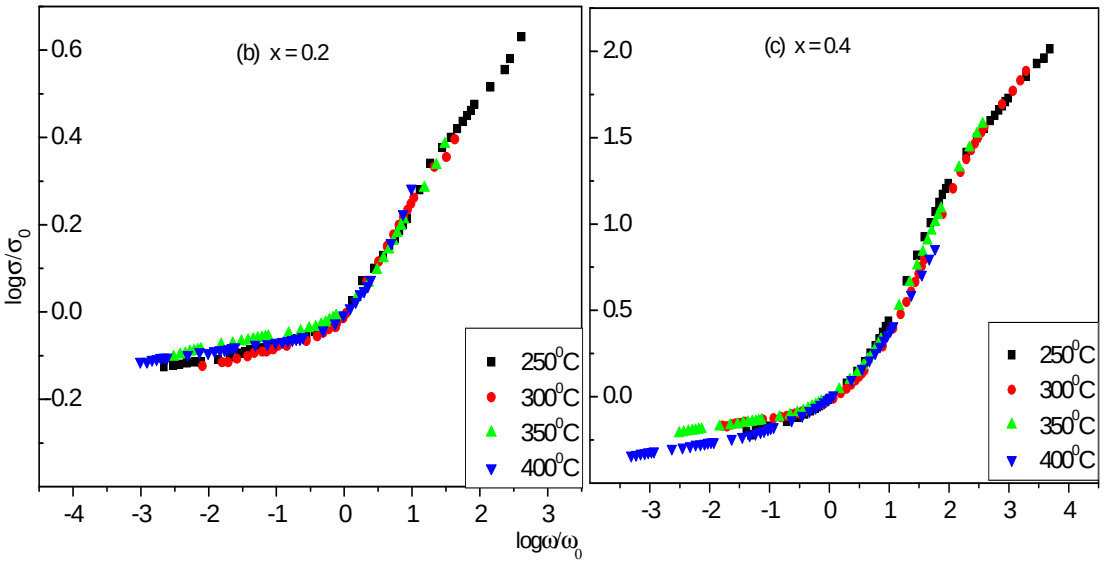

Fig.6.3 (b, c): Log ω/ω_0 vs, log σ_{ac}/σ_0 plots for (b) highest conducting and (c) lowest conducting dopant compositions of $Bi_{4-x}Ca_xV_2O_{11-\delta}$ at different temperatures.

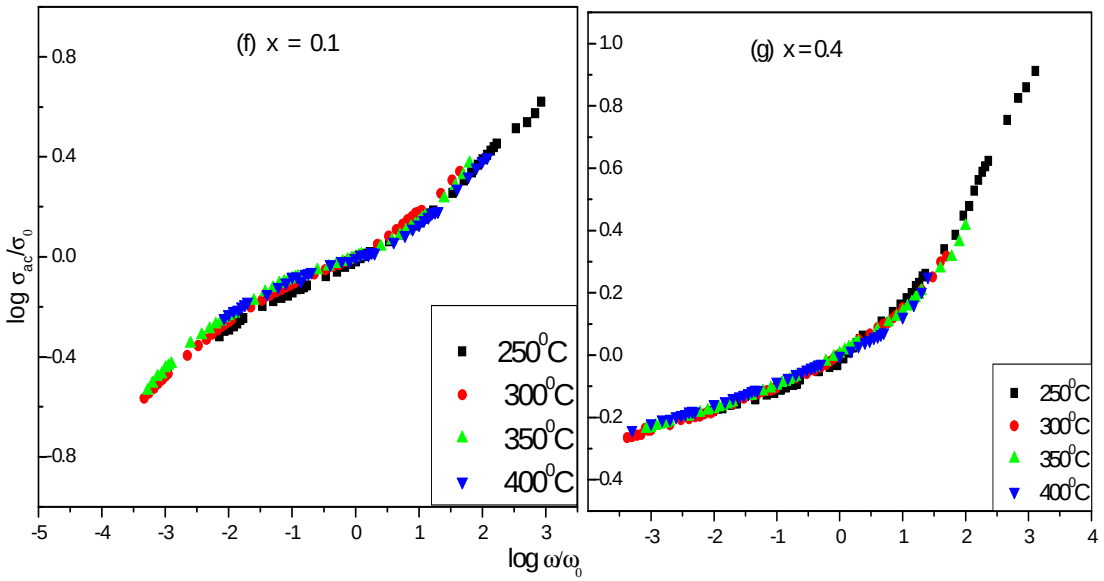

Fig.6.3 (d, e): Log ω/ω_0 vs, log σ_{ac}/σ_0 plots for (b) highest conducting and (c) lowest conducting dopant compositions of $Bi_{4-x}Ba_xV_2O_{11-\delta}$ at different temperatures.

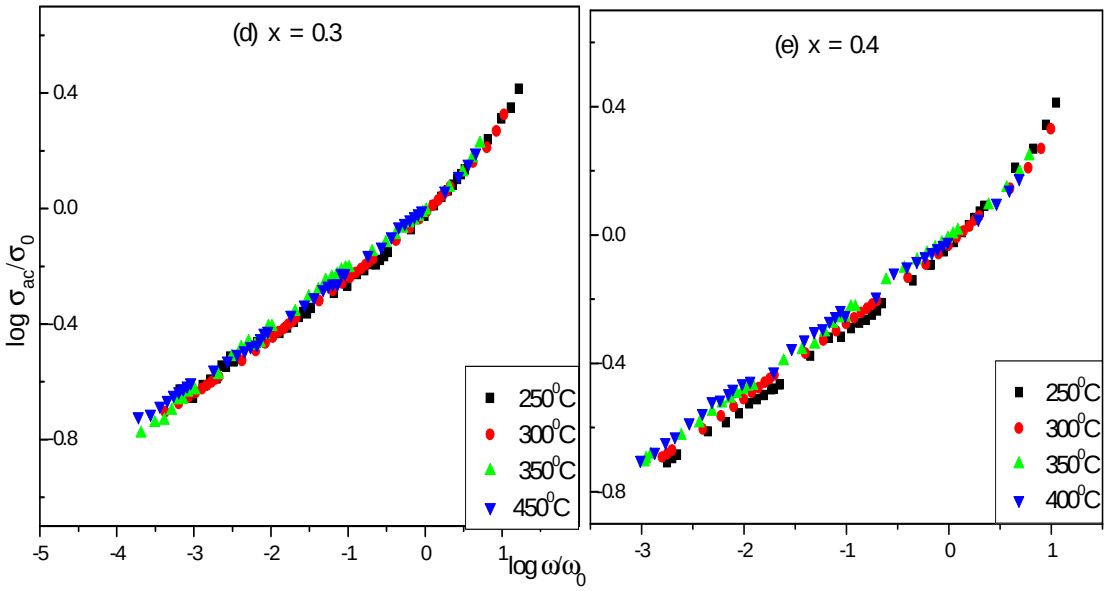

Fig.6.3 (f, g): Log ω/ω_0 vs, log σ_{ac}/σ_0 plots for (b) highest conducting and (c) lowest conducting dopant compositions of $Bi_{4-x}Li_xV_2O_{11-\delta}$ at different temperatures.

6.3.2. Electric modulus

The electric modulus data is evaluated from the real & imaginary parts of the measured impedance data and pellet dimensions respectively using the equations 1.40 & 1.41 in chapter-1 for all the three series of compositions $Bi_{4-x}Ca_xV_2O_{11-\delta}$, $Bi_{4-x}Li_xV_2O_{11-\delta}$ and $Bi_{4-x}Ba_xV_2O_{11-\delta}$. The relaxation behaviour is analyzed using the complex electric modulus ($M^* = M' + jM''$) formalism and the decay function Φ(t) given by the expression

$$\varphi(t) = exp\left[\left(\frac{-t}{\tau_\sigma}\right)^{\beta}\right] \qquad (6.2)$$

where φ(t) is the Kohlrausch–Williams–Watts (KWW) function which represents the relaxation time distribution, τ_σ is the conductivity relaxation time and β is the stretched exponent parameter [**18**].

Fig.6.4 (a-g) shows respectively the frequency dependent behaviour of imaginary part of electric modulus M" for the undoped compound, high and low conducting dopant compositions of the samples of $Bi_{4-x}Ca_xV_2O_{11-\delta}$, $Bi_{4-x}Li_xV_2O_{11-\delta}$ and $Bi_{4-x}Ba_xV_2O_{11}$ series of compounds at various temperatures.

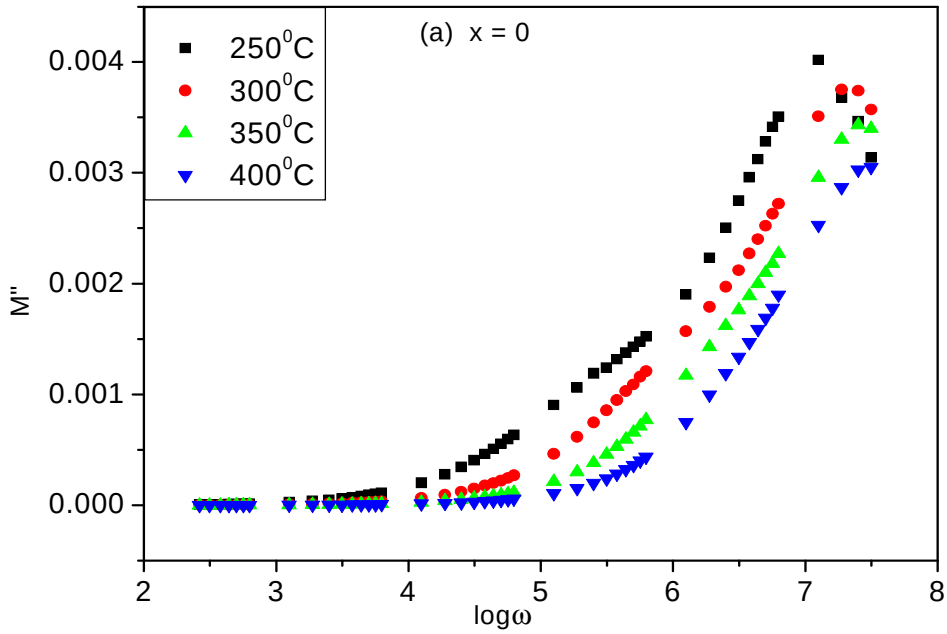

Fig.6.4 (a): Log ω vs M'' plots for the parent compound $Bi_4V_2O_{11}$ at different temperatures.

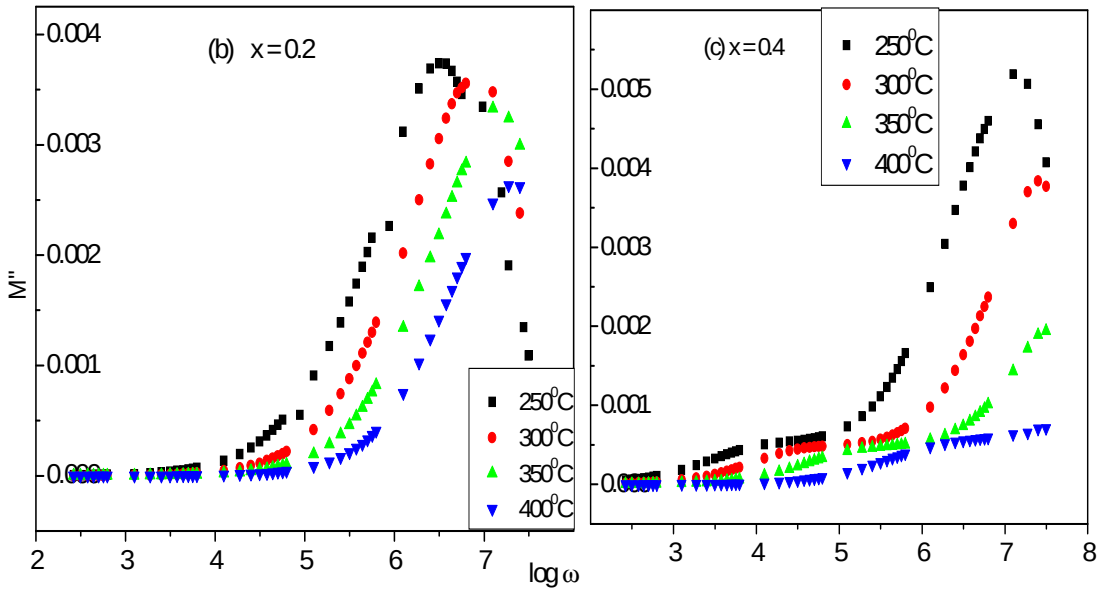

Fig.6.4 (b,c): Log ω vs M'' plots for the high and low conducting samples of the series $Bi_{4-x}Ca_xV_2O_{11-\delta}$ at different temperatures.

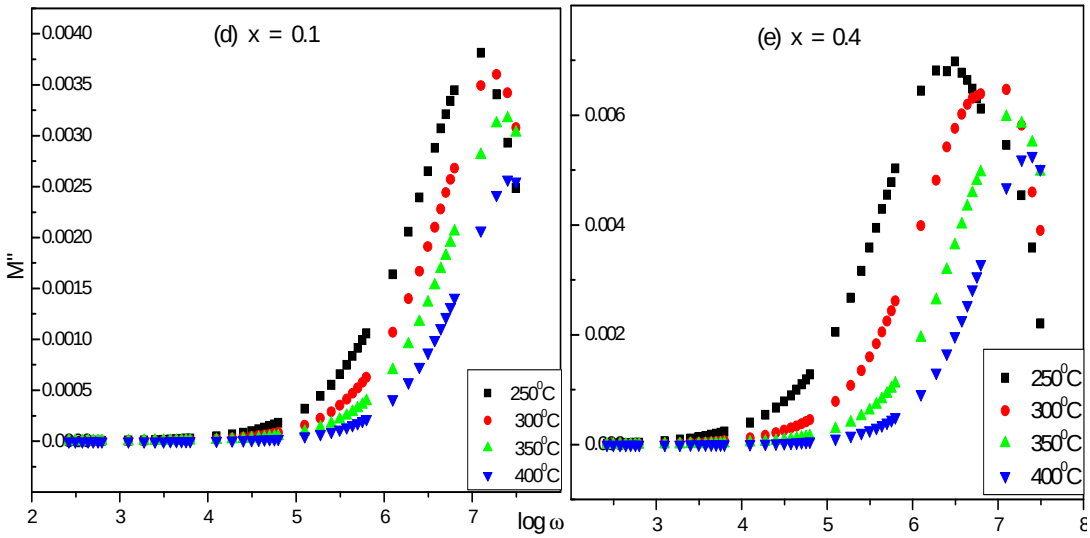

Fig.6.4 (d, e): Log ω vs M'' plots for the high and low conducting samples of the series $Bi_{4-x}Ba_xV_2O_{11-\delta}$ at different temperatures.

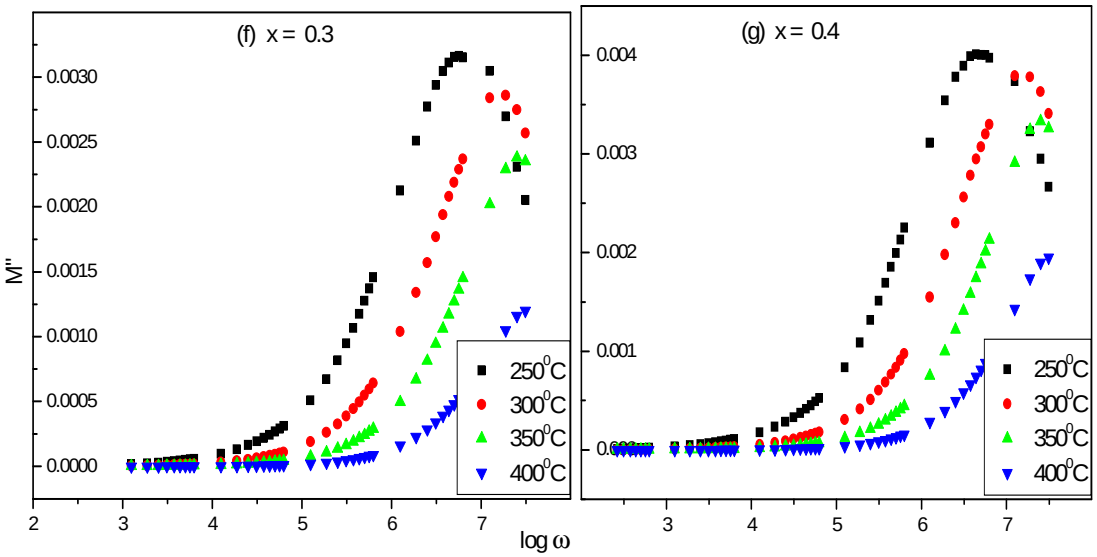

Fig.6.4 (f, g): Log ω vs M'' plots for the high and low conducting samples of the series $Bi_{4-x}Li_xV_2O_{11-\delta}$ at different temperatures.

In our present work, all the modulus studies were restricted to a temperature below 430 °C since at higher temperature the peak of the log ω vs M'' graph shifted towards higher frequency which is beyond the limit of the instrument used. It is observed that, at each temperature the imaginary part of the electric modulus is associated with a clearly resolved peak at unique frequency. The curves are asymmetric in nature

exhibited non-Debye type of behaviour. With the increase of temperature, the modulus peak maxima (ω_{max}) shift towards the high frequency region. The peaks are a sign of transition from long range to short range mobility of oxygen ions. The low frequency regions of the peak indicates temperature dependent hopping mechanism of the charge carriers over a long distance and the high frequency regions of the peak correspond to the relaxation process in which the charge carriers can make localized motion within their potential wells. [**11, 18-19**]. For x = 0.4 compound of Ca doped composition (fig3c and 4c), one more peak is observed which is diffused in nature in the low frequency side which also shifts towards high frequency region with increasing temperature.

The value of β in equation (6.2) can be calculated from the full width at half maximum (FWHM) of *log* ω versus M″ plot. By applying the method explained by Sidebottom [**20**]. The values of β are calculated by following the relation $\beta \approx 1/r$ (r is the FWHM line width in decades) and are plotted against temperature for undoped and the high conducting specimens of the respective compounds which are shown in **Fig.6.5**. It is evident from the figure that the value of β for the specimens turns out to be less than unity which confirms that the dielectric relaxation process involved in the system is non-Debye type and the compounds are primarily ionic in nature [**20**].

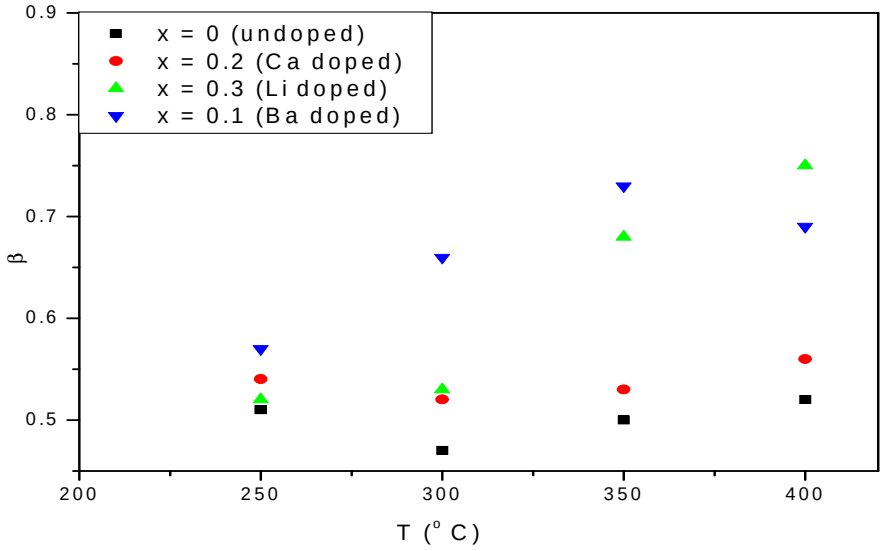

Fig.6.5: Temperature dependence of β parameter for the parent as well as the high conducting samples of the doped series of compounds.

Fig.6.6 (a-g) shows the normalized plots of electric modulus M''/M''_{max} versus log (ω/ω_{max}) for the parent as well as high conducting samples of the three series of compounds. Except for the composition x = 0.4 of Ca doped series, all the normalized plots for different temperature data overlaps and collapsed to a single master curve. This indicates that all possible relaxation mechanisms associated with different frequencies possess the same thermal energy and the corresponding dynamical processes are temperature independent [**11**].

On the other hand, in addition to the high frequency peak, the temperature curves for x = 0.4 composition of Ca-doped series (**fig.6.6c**) exhibit a diffused peak in the middle frequency region which is more pronounced at 350 °C and 400 °C. The additional peak that occur at the middle frequency region in both log ω versus M'' and log (ω/ω_{max}) versus M''/M''_{max} plots can be correlated with the dominant role played by grain boundary contribution over the bulk contribution. This is also evident from M' versus M'' plot for different compositions.

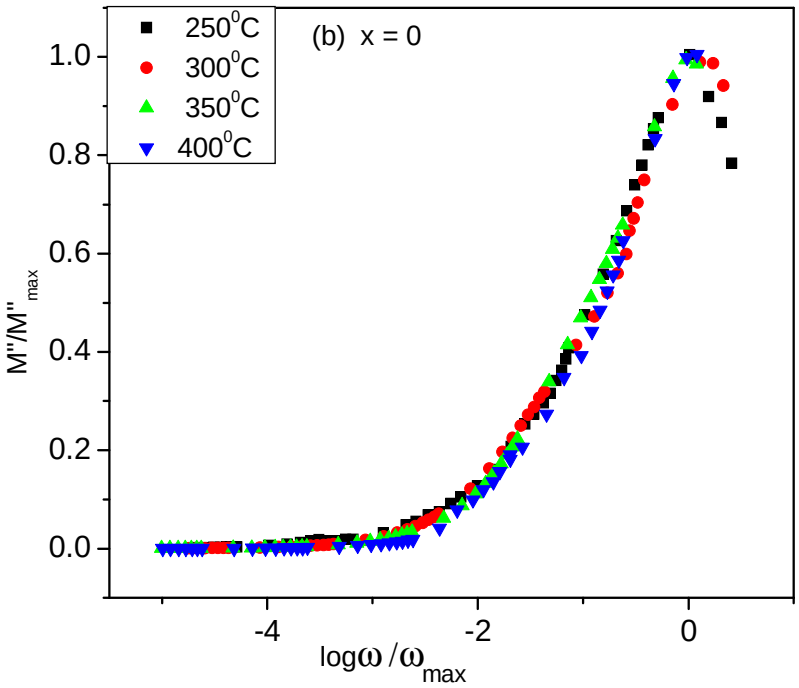

Fig.6.6 (a): M''/M''_{max} vs. log (ω/ω_{max}) plots for the parent compound $Bi_4V_2O_{11}$ at different temperatures

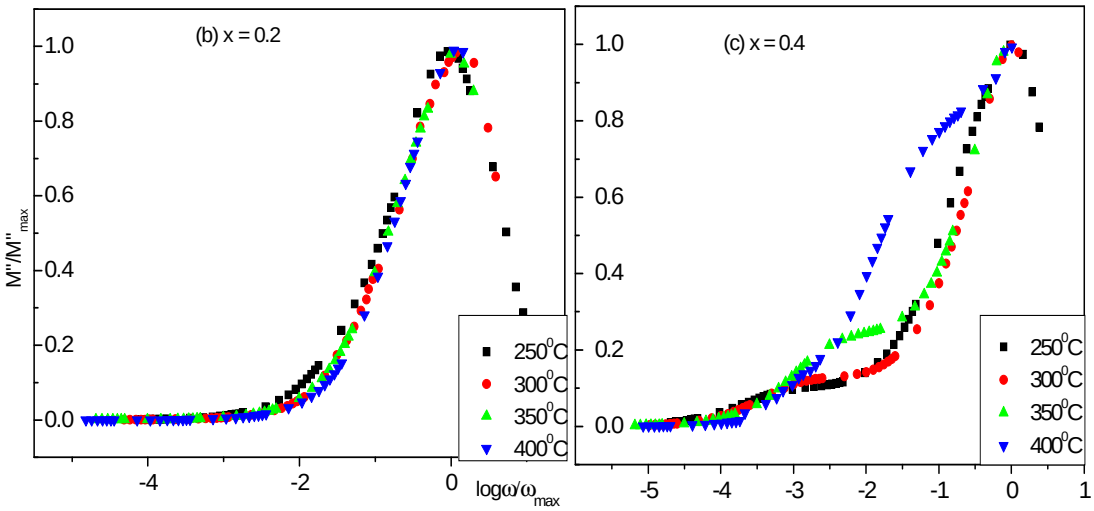

Fig.6.6 (b, c): M''/M''_{max} vs. log (ω/ω_{max}) plots for the highest and lowest conducting samples of the series $Bi_{4-x}Ca_xV_2O_{11}$ at different temperatures.

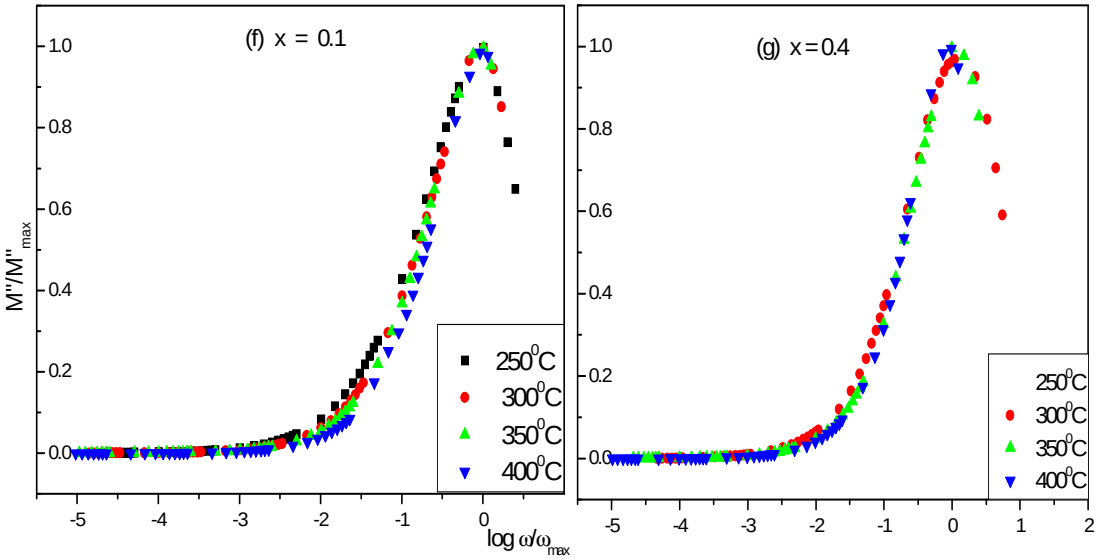

Fig.6.6 (f, g): M''/M''_{max} vs. log (ω/ω_{max}) plots for highest and lowest conducting samples of the series $Bi_{4-x}Ba_xV_2O_{11}$ at different temperatures.

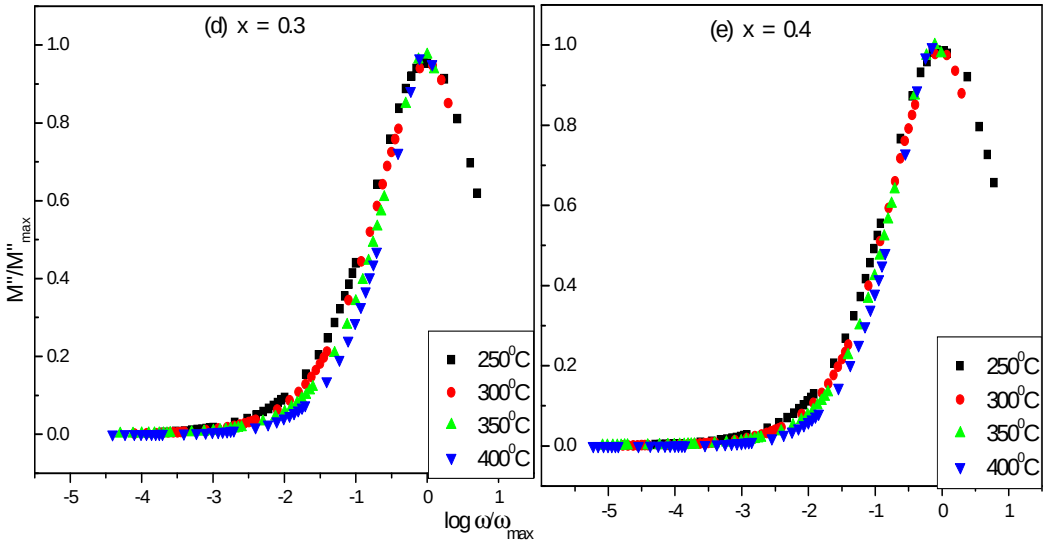

Fig.6.6 (d, e): M''/M''_{max} vs. log (ω/ω_{max}) plots for the highest and lowest conducting samples of the series $Bi_{4-x}Li_xV_2O_{11}$ at different temperatures.

A typical M' versus M'' plot at 400 °C for different compositions are shown in **Fig. 6.7**, where the peak of the plot for x = 0.4 is observed at the middle frequency range (~kHz range).

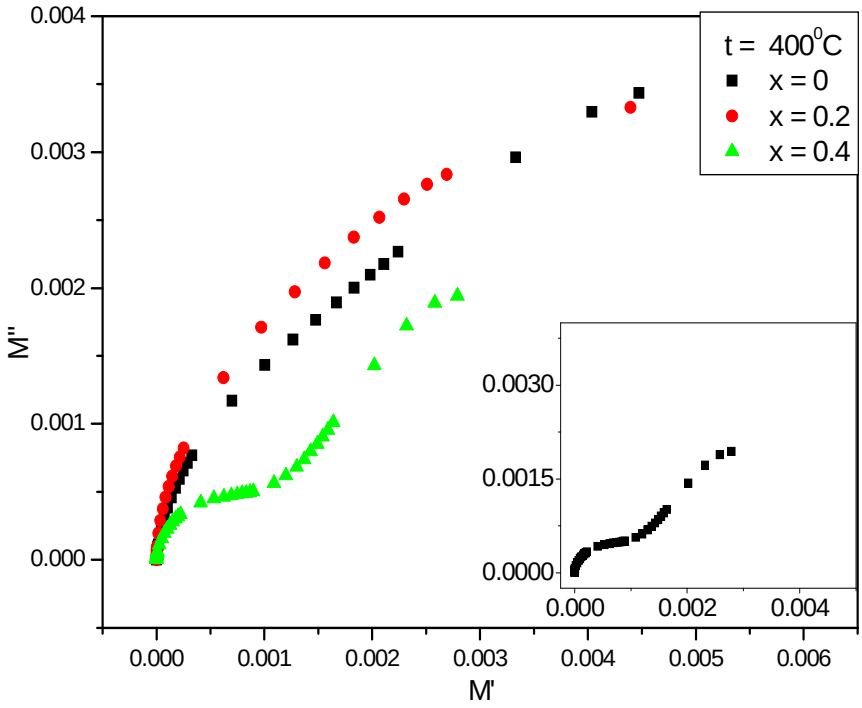

Fig. 6.7: Real modulus (M') versus imaginary modulus (M'') for x = 0, 0.2 and 0.4 compositions of $Bi_{4-x}Ca_xV_2O_{11-\delta}$ series of compound at 400 ^{0}C. Inset shows dominant grain boundary effect for x = 0.4 specimen.

It has been observed that both the hopping frequency associated with frequency dependent a.c conductivity and the modulus peak maxima (ω_{max}) shift towards the higher frequencies with increase in temperature. From these observations, it may be concluded that the conduction process within the system is associated with ion hopping mechanism [**21**].

6.4 Conclusion:

1. Polycrystalline ceramic samples of pure and doped $Bi_{4-x}Me_xV_2O_{11-\delta}$ (Me = Ca, Li, Ba) series of compounds have been synthesized by standard solid state reaction method using high purity oxides.

2. The frequency dependent conductivity (the ac conductivity) for both pure and doped compounds show three distinct regions a) low frequency dispersed b) an intermediate plateau and c) high frequency conductivity dispersion region which is typical spectrum exhibited by solid electrolyte

3. The σ_0 obtained from a.c conductivity is in good agreement with the dc conductivity obtained from the impedance analysis.

4. The value of the power law exponent 'n' ranges between 0.58 and 0.89 which lie in the range of ionic conductor.

5. The scaled behaviour of the frequency dependent conductivity suggests that the conductivity relaxation mechanism is temperature independent.

6. The imaginary part of the electric modulus is associated with a clearly resolved peak at unique frequency which shifts towards high frequency region with rhe increase of temperature.

7. The calculated values of β parameter are much less than unity which confirms that the dielectric relaxation process involved in the system is non-Debye type and the compounds are primarily ionic in nature.

8. The normalized plots of electric modulus for different temperature data indicates that relaxation mechanisms associated with different frequencies possess the same thermal energy and the corresponding dynamical processes are temperature independent

References:

[1] D.C. Graham, Chem. Rev., **41** (1947) 441.

[2] R. Parsons, Modern Aspects of Electrochemistry, Vol. 1, 1954, p. 103.

[3] P. Delahay, Double Layer and Electrode Kinetics, Wiley-Interscience, New York, 1965.

[4] D.M. Mohilner in Electroanalytical Chemistry, A.J. Bard, Ed., Dekker, New York, 1966, p.241.

[5] J. Ross Macdonald (ed) 'Impedance Spectroscopy', John Wiley & Sons, New York (1987).

[6] S.P.S.Badwal, 'Solid State Ionic Devices', Chowdari. B. V. R. , Radhakrishna S. (eds.), World Scientific, Singapore, (1988).

[7] M. D.1ngram, Phys. Chem. Glasses **18** (1987) 215.

[8] L. L. Hench, J. K. West, 'Principles of Electronic Ceramics', John Wiley & Sons, lnc. Singapore. (1990).

[9] A. K. Joncher, Phys. Thin Films **11** (1980) 231.

[10] A. K. Joncher, J. Mater. Sci. **16** (1981) 2037.

[11] S. Chouaib, A.Ben. Rhaiem, K. Guidara, Bull. Mater. Sci. **34** (2011) 915–920.

[12] D. K. Pradhan, R. N. P. Choudhary, B. K. Samantaray, eXPRESS Polymer Letters **2** (2008) 630–638.

[13] A. K. Joncher, Nature **256** (1977) 673.

[14] A. K. Joncher, 'Dielectric Relaxation in Solids', Chesla dielectric press, London, (1983).

[15] K. J. Rao, N. Baskaran, P. A**.** Ramakrishnan, B. G. Ravi, A. Karthikeyan, Chem. Mater. **10** (1998) 3109.

[16] A. H. Verhoef, H. W. Den Hartog, Solid State lonics **68** (1994) 305.

[17] S. R. Elliott, A. P. Owens, Philos. Magn. **60- 6** (1989) 777.

[18] T. Prakash, K. Padma Prasad, R. Kavitha, S. Ramasamy, B. S. Murty, J. Appl. Phys. **102** (2007) 104104(1-5).

[19] H. Mahamoud, B. Louati, F. Hlel, K.Guidara, Bull. Mater. Sci. **34** (2011) 1069–1075.

[20] D. L. Sidebottom, P. F. Green, R. K. Brow, J. Non-Cryst. Solids **183** (1995) 151-160.

[21] J. C. Dyre, Phys. Lett. **108**A, 9 (1985) 457